Published in final edited form as:

Mol Cancer Ther. 2024 April 02; 23(4): 464–477. doi:10.1158/1535-7163.MCT-23-0144.

The methyltransferases METTL7A and METTL7B confer resistance to thiol-based histone deacetylase inhibitors

Robert W. Robey[1,*], **Christina M. Fitzsimmons**[1,*], **Wilfried M. Guiblet**[1,8], **William J.E. Frye**[1], **José M. González Dalmasy**[1], **Li Wang**[2], **Drake A. Russell**[3], **Lyn M. Huff**[1], **Andrew J. Perciaccante**[1], **Fatima Ali-Rahmani**[1,9], **Crystal C. Lipsey**[1], **Heidi M. Wade**[1], **Allison V. Mitchell**[1], **Siddhardha S. Maligireddy**[1], **David Terrero**[4], **Donna Butcher**[5], **Elijah F. Edmondson**[5], **Lisa M. Jenkins**[1], **Tatiana Nikitina**[1], **Victor B. Zhurkin**[1], **Amit K. Tiwari**[4], **Anthony D. Piscopio**[6], **Rheem A. Totah**[3], **Susan E. Bates**[7], **H. Efsun Arda**[2], **Michael M. Gottesman**[1,#], **Pedro J. Batista**[1,#]

[1]Laboratory of Cell Biology, Center for Cancer Research, National Cancer Institute, National Institutes of Health, Bethesda, MD

[2]Laboratory of Receptor Biology and Gene Expression, Developmental Genomics Group, Center for Cancer Research, National Cancer Institute, National Institutes of Health, Bethesda, MD

[3]Department of Medicinal Chemistry, University of Washington, Seattle, WA

[4]Department of Pharmacology and Experimental Therapeutics, Department of Cancer Cell and Cancer Biology, University of Toledo, Toledo, OH

[5]Molecular Histopathology Laboratory, Frederick National Laboratory for Cancer Research, Frederick, MD, USA

[6]OnKure, Inc., Boulder CO

[7]Division of Hematology/Oncology, Department of Medicine, Columbia University Medical Center, New York, NY and Hematology/Oncology Research Department, James J. Peters Department of Veterans Affairs Medical Center, New York, NY

[8]Present address: Advanced Biomedical Computational Science, Frederick National Laboratory for Cancer Research, Frederick, MD

[9]Present Address: Taiho Pharmaceutical, Princeton, NJ

Abstract

Histone deacetylase inhibitors (HDACis) are part of a growing class of epigenetic therapies used for the treatment of cancer. Although HDACis are effective in the treatment of T-cell lymphomas, treatment of solid tumors with this class of drugs has not been successful. Overexpression of the multidrug resistance protein P-glycoprotein (P-gp), encoded by *ABCB1*, is known to confer

[#]To whom correspondence should be addressed: pedro.batista@ni.gov National Institutes of Health, 37 Convent Drive, Building 37 Room 2128, Bethesda, MD 20892 and gottesmm@mail.nih.gov National Institutes of Health, 37 Convent Drive, Building 37 Room 2108, Bethesda, MD 20892.

[*]These authors contributed equally to this work.

Authors' Discosures: Anthony D. Piscopio is CEO and president of OnKure, Inc. The other authors declare no potential conflicts of interest.

resistance to the HDACi romidepsin *in vitro*, yet increased *ABCB1* expression has not been associated with resistance in patients, suggesting that other mechanisms of resistance arise in the clinic. To identify alternative mechanisms of resistance to romidepsin, we selected MCF-7 breast cancer cells with romidepsin in the presence of the P-gp inhibitor verapamil to reduce the likelihood of P-gp-mediated resistance. The resulting cell line, MCF-7 DpVp300, does not express P-gp and was found to be selectively resistant to romidepsin but not to other HDACis such as belinostat, panobinostat, or vorinostat. RNA sequencing analysis revealed upregulation of the mRNA coding for the putative methyltransferase, *METTL7A*, whose paralog, *METTL7B*, was previously shown to methylate thiol groups on hydrogen sulfide and captopril. As romidepsin has a thiol as the zinc-binding moiety, we hypothesized that METTL7A could inactivate romidepsin and other thiol-based HDACis via methylation of the thiol group. We demonstrate that expression of METTL7A or METTL7B confers resistance to thiol-based HDACis and that both enzymes are capable of methylating thiol-containing HDACis. We thus propose that METTL7A and METTL7B confer resistance to thiol-based HDACis by methylating and inactivating the zinc-binding thiol.

Keywords

Drug resistance; histone deacetylase; methyltransferase; romidepsin; thiol

INTRODUCTION

Post-translational modification of histone tails via methylation, phosphorylation, or acetylation is an essential aspect of gene regulation in the cell (1). Histone acetylation is controlled by histone acetyltransferases (HATs), which catalyze the addition of acetyl groups to histones, and histone deacetylases (HDACs), which catalyze their removal. Several HDAC inhibitors (HDACis) (Supplemental Figure S1) have been developed that reversibly block histone deacetylation by coordinating with Zn^{2+} in the catalytic pocket of HDACs, thus resulting in increased histone acetylation via unrestrained HAT activity (2). The United States Food and Drug Administration (FDA) has approved two HDACis, vorinostat and romidepsin, as single agents for the treatment of cutaneous T-cell lymphoma (3-6). Additionally, belinostat received FDA approval as a single agent for the treatment of peripheral T-cell lymphoma (7) and tucidinostat (chidamide) has been approved in China for the same indication (8). Romidepsin is unique among the HDACis that have been approved for cancer treatment in that it is a bicyclic depsipeptide with an internal disulfide bond that must be reduced to form the activated molecule (9).

While romidepsin treatment is effective in some T-cell lymphoma patients, some patients present with resistant disease. In addition, clinical trials involving solid tumors were unsuccessful (10), suggesting intrinsic resistance mechanisms. Romidepsin was identified as a substrate of the ATP binding cassette transporter P-glycoprotein (P-gp, encoded by the *ABCB1* gene) based on studies with the NCI-60 cell lines, and several groups have reported overexpression of P-gp in cell lines that are selected for resistance to romidepsin (11-15). However, *ABCB1* expression in clinical samples did not predict response to romidepsin (16), prompting us to search for non-P-gp mechanisms of resistance.

To identify other potential mechanisms of romidepsin resistance, MCF-7 breast cancer cells were selected with romidepsin and verapamil, a P-gp inhibitor, to prevent emergence of P-gp as a resistance mechanism. The resulting cell line, MCF-7 DpVp300, was selectively resistant to romidepsin in the absence of P-gp expression. One of the top ten genes found to be overexpressed in the MCF-7 DpVp300 line by RNA sequencing (RNA-seq) was *METTL7A*, a putative methyltransferase. This gene was also overexpressed in the HuT78 DpVp50 line that we characterized previously (17), We pursued METTL7A as a resistance mechanism since METTL7B, a close homolog, was shown to methylate thiol groups on drugs such as captopril (18). Methylation of the zinc-binding thiol of romidepsin is known to inactivate the drug (9). Here, we demonstrate that METTL7A overexpression confers resistance to all HDACis tested that have a thiol as the zinc-binding moiety. METTL7B also confers resistance to thiol-containing HDACis, albeit with less efficiency. Overexpression of these methyltransferases represents a previously unknown mechanism of resistance to thiol-based HDACis and a potential target to improve HDACi-based therapies.

MATERIALS AND METHODS

Chemicals

Methotrexate, 5-fluoruracil, teniposide, apicidin, trichostatin A, and topotecan were obtained from Sigma Aldrich (St. Louis, MO, RRID:SCR_008988). Romidepsin was obtained from Selleck Chem (Houston, TX, RRID:SCR_003823). Belinostat, mocetinostat, and panobinostat were purchased from ChemieTek (Indianapolis, IN). Dacinostat, resminostat, pracinostat, chidamide, vorinostat, entinostat, NCH-51, and KD 5170 were obtained from Cayman Chemical (Ann Arbor, MI, RRID:SCR_008945). Rocilinostat was purchased from ApexBio Technology (Houston, TX). PCI-34051 was from Tocris (Minneapolis, MN, RRID:SCR_003689). The phenylethanolamine-N-methyltransferase inhibitor 2,3-Dichloro-α-methylbenzylamine hydrochloride (DCMB) was obtained from Santa Cruz Biotechnology (Dallas, TX, RRID:SCR_008987). Largazole and OKI-005 were synthesized by OnKure (19-21).Chemical structures for romidepsin, largazole, OKI-005, NCH-51 and KD-5170 as well as all non-FDA approved agents used in this study are shown in Supplemental Figure S1.

Cells

MCF-7 breast cancer cells were obtained from Dr. Marc Lippman (National Institutes of Health, National Cancer Institute) and were selected with romidepsin to generate the MCF-7 DpVp300 cell line that is maintained in 300 ng/ml romidepsin with 5 μg/ml verapamil. The HuT78 cell line was purchased from ATCC (Manassas, VA, RRID:CVCL_0337) and the romidepsin-resistant HuT78 DpVp50 and DpP75 cell lines have been previously described (17). All cells were cultured in RPMI-1640 supplemented with 10% FCS and penicillin-Streptomycin (Pen-Strep). HEK293 cells (ATCC, RRID:CVCL_0045) were maintained in Eagle's minimum essential medium with 10% FCS and Pen-Strep. HEK293 cells were transfected with empty pcDNA3.1 vector, or vector containing full-length *METTL7A* or *METTL7B* with a C-terminal FLAG tag (all vectors from Genscript, Piscataway, NJ) using Lipofectamine 2000 (ThermoFisher Scientific, Waltham, MA) according to the manufacturer's instructions. Clones were selected and maintained in 1 mg/mL G418.

CRISPR-mediated knockout of METTL7A from MCF-7 DpVp300 cells was achieved by co-transfecting knockout and homology directed repair vectors for *METTL7A* (Santa Cruz Biotechnology, Dallas, TX) using Lipofectamine 2000 and subsequent selection with puromycin (3 μg/ml). Clones were then isolated and characterized for loss of METTL7A protein via immunoblot. Cell lines were authenticated by STR analysis (ATCC) and experiments were performed within six months after authentication. Cells were checked for mycoplasma every six months using the MycoAlert PLUS kit (Lonza, Walkersville, MD, RRID:SCR_000377).

Cytotoxicity assays

Cells were plated at a density of 5000 cells per well in opaque, white 96-well plates and allowed to attach overnight. The next day drugs were added, and plates were incubated for 3 days after which CellTiterGlo (Promega, Madison, WI) was added according to the manufacturer's instructions. Plates were read on a Tecan Infinite M200 Pro (Tecan Systems, Inc., San José, CA, RRID:SCR_019033).

Immunoblot analysis

Whole cell lysates were obtained by harvesting cells in RIPA buffer and sonicating samples in an inverted cup horn sonicator for 3 bursts of 30 sec, after which the samples were centrifuged at 9500 x g for 10 min and soluble proteins were removed. When examining histone acetylation, RIPA buffer additionally contained 500 nM trichostatin A to inhibit histone deacetylases. Protein lysates (approx. 15-20 μg) were separated by PAGE, and transferred to nitrocellulose membranes, and subsequently probed with antibodies against total histone H3 (cat# 05-499, Millipore-Sigma, Burlington, MA, RRID:AB_309763), pan-Acetyl histone H3 (cat# 06-599, Millipore-Sigma, RRID:AB_2115283), METTL7A (cat# TA346478, Origene, Rockville, MD, RRID:AB_3076201), METTL7B (cat# HPA830644, Millipore-Sigma, RRID:AB_2676130), beta-actin, (generated in mouse cat# 3700 RRID:AB_2242334; or rabbit cat# 4970, RRID:AB_2223172; both from Cell Signaling Technology, Danvers, MA) and p21 (cat# 2946, Cell Signaling, RRID:AB_2260325). Anti-FLAG antibody (cat# F1804-200UG, RRID:AB_262044) was from also from Millipore-Sigma.

Flow cytometry

To determine surface expression of P-glycoprotein, trypsinized cells were incubated with phycoerythrin-labeled UIC2 antibody (ThermoFisher, Grand Island NY, RRID:AB_1603172) or phycoerythrin-labeled isotype control IgG2a kappa (ThermoFisher, Grand Island, NY, RRID:AB_1603322) for 20 min at room temperature in 2% bovine serum albumin in phosphate buffered saline (PBS). Cell fluorescence was measured with a FACS Canto flow cytometer (BD Biosciences, San José, CA, RRID:SCR_018055) and data analysis was performed using FlowJo v10.4.2 (FlowJo LLC, Ashland OR, RRID:SCR_008520). At least 10,000 events were collected per sample. For cell cycle analysis, cells were plated and allowed to attach overnight before being treated with HDACis for 24 h. Cells were then harvested by trypsinization, centrifuged, and the supernatant removed. Cell pellets were resuspended in equal volumes of staining solution (0.05 mg/ml propidium iodide and 0.1% Triton X) and RNAse A solution (200 U/mL RNAse A in

deionized water). Cells were stained for 20 min and were subsequently read on a FACS Canto Flow Cytometer with at least 10,000 events collected per sample. The percentage of cells in each phase of the cell cycle was determined by Modfit LT for Mac version 5.0 (Verity Software House, Topsham, ME, RRID:SCR_016106). Statistically significant changes in the percent of cells in each phase of the cell cycle were determined by a one-way ANOVA test with a correction for multiple comparisons.

RNA sequencing analysis

RNA was extracted from the MCF-7, MCF-7 DpVp300, HuT78, and HuT78 DpVp50 cell lines using the RNeasy kit from Qiagen (Germantown, MD). RNA sample integrity and quantity for three biological replicates were assessed by the Center for Cancer Research (CCR) Genomics Core using RNA ScreenTape Analysis (Agilent). RNA libraries were generated using a TruSeq Stranded mRNA library prep kit (Illumina) and paired-end RNA sequencing (2 x 75) was performed by the CCR Sequencing Facility and Genomics Technology Core (RRID:SCR_024754) on a NextSeq 500 Sequencing System (RRID:SCR_014983). Read quality analysis was performed using FASTQC (RRID:SCR_014583). Reads were trimmed for adapters and low-quality bases using Cutadapt (version 2.3, RRID:SCR_011841) before alignment with the hg38 reference genome using Spliced Transcripts Alignment to a Reference (version 2.7.0f, RRID:SCR_004463). The number of reads mapping to each transcript was determined with HTseq-count (version 0.9.1, RRID:SCR_011867). Differential expression was determined using DESeq2 (version 1.26.0, RRID:SCR_015687) within R(version 3.6.3, RRID:SCR_001905).

Omni-ATAC-seq assay and library analysis.

Approximately 20,000 cells per sample were used for omni ATAC-seq assay following the protocol described in Corces et al. (22) with minor modifications. For each cell line, two biological replicates were included for control and resistant lines, respectively. To isolate the nuclei, cells were resuspended in cold ATAC-Resuspension Buffer (RSB) containing 0.1% NP40, 0.1% Tween-20, and 0.01% Digitonin, and incubated on ice for 3 minutes. The lysis was washed by addition of 1 mL of RSB containing 0.1% Tween-20 and mixed by inverting tubes. Nuclei were then pelleted at 500 x *g* for 10 minutes at 4°C. For transposition, each pellet was resuspended in 50 µL of transposition mix (25 µl 2x TD buffer, 2.5 µl transposase (100 nM final), 16.5 µl PBS, 0.5 µl 1% digitonin, 0.5 µl 10% Tween-20, 5 µl H_2O) and incubated at 37°C for 30 minutes in a thermomixer with 1000 rpm shaking. After transposition, reactions were stopped by adding EDTA to a final concentration of 40 mM. Transposed DNA fragments were purified using Zymo DNA Clean and Concentrator-5 Kit (cat# D4014) and PCR amplified for 5 cycles. Each PCR reaction contained 2.5 µl of 25 µM i5 primer, 2.5 µl of 25 µM i7 primer, 25 µl 2X NEBNext high-fidelity master mix (New England Biolabs #M0541), and 20 µl transposed or cleaned DNA sample. PCR conditions were as follows: 72°C for 5 min, 98°C for 30 sec, followed by 5 cycles of [98°C for 10 sec, 63°C for 30 sec, 72°C for 1 min] and then kept at 4°C. PCR reactions were purified using the Zymo kit. The purified ATAC libraries were quantified on an Aligent TapeStation using D5000 high sensitivity tapes and mixed at an equal molar ratio. The library pool was then size-selected for 100-1000 bp on a 1% agarose gel. The final library was sequenced

on Illumina NextSeq2000 (RRID:SCR_023614) for a 100 bp pair-ended run to obtain 100 million reads per sample. FASTQ files were processed using the PEPATAC (v 2.0.0) pipeline (RRID:SCR_024758) (23) against the hg38 build of the human genome. Differently accessible regions were determined using DESeq2 (version 1.26.0) within R (version 3.6.3). *De novo* and known motif enrichment analysis was performed with HOMER (24) (RRID:SCR_010881). To identify potential regulators of METTL7A transcription in DpVp cells, we computed a list of transcription factor (TF) binding sites in the promoter region of METTL7A, identified through differential peak analysis between parental and DpVp cells (chr12:50922687-50926213), using CIS-BP (http://cisbp.ccbr.utoronto.ca/TFTools.php) (25) (RRID:SCR_017236) with the parameters Motif model: PWMs – LogOdds and Threshold 8. For each TF in this list, we extracted the log2 fold change (l2fc) expression levels from RNA-seq.

Chromatin extraction and MNase+ExoIII-seq assay

Cells were harvested at 80% confluency using a cell scraper, centrifuged at 125 x g for 5 min and washed once with cold PBS. Cells were then resuspended in cold RSB buffer (10 mM Tris-HCl, pH 8.0, 10 mM NaCl, 3 mM $MgCl_2$) containing 0.5% Nonidet P-40, 1 mM PMSF and put on ice. The cell suspensions were homogenized by 20 strokes of pestle B in a Dounce homogenizer over 30 min on ice. Released nuclei were centrifuged in Sorvall X Pro centrifuge at 150 x *g*, 4°C for 5 min. The nuclei pellet was then resuspended in cold RSB buffer supplemented with 1 mM PMSF.

Before digestion, $1x10^6$ nuclei in RSB buffer with 1 mM PMSF were supplemented with 2 mM $CaCl_2$ and kept at 37°C for 5 min. 5 units of Micrococcal nuclease (Nuclease S7 Micrococcal Nuclease, cat# 10107921001; Roche Applied Science via Millipore-Sigma) with 200 units ExoIII (cat# M0206S; New England Biolabs, Ipswich, MA) were added to each nuclei aliquot and incubated for 10 min at 37°C. The reactions were stopped by adding EDTA to a final concentration of 5 mM. Digested nuclei were centrifuged at 4,600 x g in a Sorvall Legend Micro tabletop centrifuge. The supernatant S1 was removed and discarded, and the pellet was resuspended in cold TE buffer, (10 mM Tris-HCl pH 8.0, 1 mM EDTA), gently pipetted and incubated on ice for 10 min. After centrifugation, supernatant S2 was collected, pelleted material was resuspended in TE buffer, and after third centrifugation supernatant S3 was collected. Supernatants 2 and 3 were analyzed on 1% agarose gel in TAE buffer to confirm the release of DNA fragments, then combined and treated with 1% SDS and 20 μg of proteinase K (New England Biolabs, #P8107S). The reaction was incubated for 1 h at 55°C. DNA was extracted with phenol-chloroform-isoamyl alcohol, precipitated in 2.5 volumes of 100% alcohol supplemented with 50 mM sodium-acetate and precipitated at −80°C overnight. Samples were centrifuged at 17,000 x *g* at a tabletop centrifuge, pellet was rinsed in 70% alcohol, air dried and dissolved in TE buffer (10 mM Tris-HCl, pH 8.0, 0.2 mM EDTA). Total DNA was sequenced on Illumina NextSeq2000 for a 100 bp pair-ended run to obtain 300 million reads per sample.

LC-MS to detect methylated romidepsin in culture medium

Media was centrifuged 5000 × *g* for 15 minutes to pellet insoluble material and 50 μL of supernatant was removed for mass spectrometry analysis. For each, 10 μL was injected on

an Exion liquid chromatography system (SCIEX, Framingham, MA) coupled inline to an X500B QTOF mass spectrometer (SCIEX, Framingham, MA) in-line with an Exion liquid chromatography system (SCIEX, Framingham, MA). Each sample was separated on a 2.1 x 50 mm Aeris 3.6 μm WIDEPORE XB-C8 200 Å column (Phenomenex, Torrance, CA) at 0.3 mL/min using a 4 min linear gradient from 98% A (0.1% formic acid) to 40% B (acetonitrile with 0.1% formic acid). Data was acquired in positive mode over a mass range of 100-800 m/z with data dependent acquisition MS/MS performed over the mass range of 50-750 m/z. Relative quantitation was performed from extracted ion chromatogram peak areas using SCIEX OS software (SCIEX, Framingham, MA, RRID:SCR_023651).

Reduction of romidepsin

Romidepsin was added to 1 mL of deoxygenated 50 mM Tris-HCl buffer pH 7.5 with 10 mM TCEP. The final romidepsin concentration was 1 mM and was incubated at 37 °C for 1.5 h in the TCEP-containing, buffered solution. At 1.5 h the romidepsin, now almost completely reduced, was extracted with 1X ethyl acetate. Briefly, 1mL of ethyl acetate was added to the 1 mL solution of, now reduced, romidepsin. The entire solution was vortexed, centrifuged briefly at 5000 x *g*, and then incubated at −80 °C to freeze the aqueous components. The top layer of ethyl acetate does not freeze and was transferred to a new vial and dried with a slow stream of nitrogen gas. The dried reduced romidepsin was then reconstituted with acetonitrile.

Synthesis of (D3)2-diemthyl-romidepsin

We determined that, when reduced with TCEP as previously described, romidepsin was almost completely converted to the reduced form. We therefore assumed that when reconstituted with acetonitrile, the solution contains approx. 1 μmol of reduced romidepsin. All reagents are added based on this estimated yield of reduced romidepsin. To a solution of acetonitrile containing 1 μmol of reduced romidepsin dissolved in acetonitrile, 10 μmol of N,N-Diisopropylethylamine (DIPEA) and 5 μmol of D3-iodomethane were added. The solution was incubated at room temperature for 2 h before adding a small volume of water to quench the remaining iodomethane. The solution was then dried down with a slow stream of nitrogen gas. The dried D3-dimethyl-romidepsin was then reconstituted with acetonitrile and stored at −80 °C.

Romidepsin methylation activity with purified enzyme

Purified N-GST-METTL7A and -METTL7B were individually diluted to 0.2 mg/mL in KPi reaction buffer (50 mM KPi pH 7.0, 20% glycerol, 150 mM NaCl, 10 mM CHAPS). The diluted purified thiol methyltransferases were then added 1:2 to a solution of 9 mg/mL 1,2-Dimyristoyl-sn-glycero-3-phospho-rac-(1-glycerol) sodium salt (DMPG) dissolved in KPi reaction buffer. The final protein concentration was 0.07 mg/mL for each protein. The solutions of diluted protein were incubated on ice for 30 mins. Small volumes of diluted METTL7A and METTL7B were then aliquoted into separate vials and boiled for 5 min to inactivate the enzymes. A small volume of reduced romidepsin was deposited into relevant wells of a 96-well reaction plate. The acetonitrile solvent was removed by placing the plate in a vacuum chamber and pulling a vacuum for several minutes. The diluted proteins were added to the plate wells containing dried reduced romidepsin. Vehicle control was then

added to relevant wells containing the diluted thiol methyltransferases. The well plate was allowed to shake at 625 rpm on a plate shaker for 5 min. Finally, SAM or a vehicle control of liquid chromatography-grade water was added to the appropriate wells to initiate the reaction. The final concentration of protein was 0.06 mg/mL and the final concentration of SAM was 500 μM. The estimated final concentration of reduced romidepsin was approx. 500 μM. After SAM was added to initiate the reaction, the samples were incubated at 37 °C for 2 h. After 2 h, ice-cold acetonitrile containing the (D3)2-dimethyl-romidepsin internal standard was added to precipitate salts and proteins at a ratio of 3:7 (reaction volume:MeCN). The plate was centrifuged at 5000 x *g* for 20 min and then the supernatant from each well was transferred to a new well in a 96-well plate for LC-MS analysis.

Immunohistochemistry

Serial sections from normal tissue microarrays (BCN921 and BN1021) were obtained from tissuearray.com (Derwood, MD) and serial sections from a T-cell lymphoma array (LYM1503) were obtained from Pantomics (Fairfield, CA). Slides were immunolabeled for METTLA and METTLB according to conditions in Supplemental Table S1. Serial sections were also stained with a negative control protocol in which primary antibody was replaced by nonclonal antibody from the same species and of the same isotypes (isotype controls). Positive controls included cell pellet slides with known expression of METTL7A (7A 1-2, 7A 1-4) and METTL7B (7B 1-3, 7B 2-2). Slides were analyzed and manually evaluated for positive staining along with negative controls; positive cell types were listed and assigned a semi-quantitative grade for positivity (minimal, mild, moderate, or marked; 1+, 2+, 3+, 4+). Slides were also digitalized and analyzed using QuPath (v 0.3.2) (RRID:SCR_018257) (26). Digital image analysis included identifying stain vectors, de-arraying tissue microarrays, defining regions of interest, cell detection, and quantifying chromogenic immunohistochemistry staining. Following automated TMA grid detection, manual pathologist review was performed to exclude spots or regions of spots that were non-assessable, non-tumor containing (in the case of the T-cell lymphoma array) or obscured by artifact. For the T-cell lymphoma array, duplicate cores, where present, were averaged and a positivity threshold of 5% of cells was used to differentiate.

Data and code availability

RNA-seq and ATAC-seq data were deposited in the Gene Expression Omnibus database (RRID:SCR_005012) at GSE217130. Code and scripts used to generate data and plots are available at https://github.com/BatistaLab/METTL7A

RESULTS

MCF-7 DpVp300 cells are selectively resistant to romidepsin

The MCF-7 DpVp300 cell line was generated via prolonged selection of MCF-7 cells with romidepsin in the presence of the P-gp inhibitor verapamil to prevent any benefit from P-gp overexpression. To determine the cross-resistance profile of MCF-7 DpVp300 cells, cytotoxicity assays were performed with several chemotherapeutic agents (Supplemental Figure S1). Interestingly, the DpVp300 cell line was much more resistant to romidepsin (Figure 1A, approx. 218-fold resistant) compared to other HDACis, such as belinostat

(8-fold), panobinostat (2.5-fold), and vorinostat (5-fold). Additionally, the MCF-7 DpVp300 line was not cross resistant to other chemotherapeutic agents such as 5-FU, methotrexate, teniposide, or topotecan, exhibiting no more than 3-fold resistance to those compounds than MCF-7 cells (Supplemental Table S2).

As HDACi treatment typically results in increased levels of acetylated histones and p21 (27) , we examined the effect of romidepsin, belinostat, panabinostat or vorinostat treatment on parental and resistant cells. MCF-7 cells displayed increased levels of acetylated histone H3 and p21 after treatment with all of the HDACis compared to untreated cells (Figure 1B). In contrast, MCF-7 DpVp300 cells treated with romidepsin did not exhibit increased levels of acetylated histone H3 or p21; however, treatment with the other HDACis resulted in high levels of acetylated histone H3, which suggested a resistance mechanism that is specific to romidepsin and acts upstream of the deacetylation process.

Treatment of cancer cell lines with HDACis is known to cause cell cycle perturbations, with some cell lines demonstrating a G_1/G_0 arrest and others a G_2/M arrest (28-30). In MCF-7 cells treated with HDACis, we observed a decrease in the percentage of cells in the G_1/G_0 and S phases and an increase in cells in the G_2/M phase (Figure 1C and Supplemental Figure S2A). While a similar pattern was observed in MCF-7 DpVp300 cells when treated with belinostat, panobinostat or vorinostat, no cell-cycle changes were observed with romidepsin treatment (Figure 1C and Supplemental Figure S2A).

To examine dose-dependent effects, we treated MCF-7 and DpVp300 cells with increasing concentrations of romidepsin. While MCF-7 cells displayed increased levels of histone H3 acetylation and p21 when treated with as little as 1 ng/ml romidepsin, this was not observed until MCF-7 DpVp300 cells were treated with 100 ng/ml romidepsin (Figure 1D). Based on these results, we concluded the resistance mechanism present in MCF-7 DpVp300 cells protected the cells from romidepsin levels at least 100 times higher than MCF-7 cells – consistent with the earlier observation in cytotoxicity assays that MCF-7 DpVp300 cells are at least 200-fold resistant to romidepsin (Figure 1A).

P-gp is not responsible for romidepsin resistance in MCF-7 DpVp300 cells

We and others have demonstrated that selection with romidepsin alone leads to overexpression of P-gp as a resistance mechanism (12,14,15,31). To confirm that P-gp does not play a role in romidepsin resistance in the DpVp300 cell line, we measured surface expression of P-gp by flow cytometry. While P-gp was readily detected in the *ABCB1*-transfected MDR-19 cell line, P-gp was undetected in the empty vector transfected line, MCF-7, or MCF-7 DpVp300 cells. Resistance to romidepsin in the MDR-19 line compared to empty vector transfected cells leads to approximately the same degree of resistance as that observed between DpVp300 cells and MCF-7 cells (Supplemental Figure S2C). Thus, we concluded the mechanism of resistance at work in the MCF-7 DpVp300 cells is P-gp-independent.

MCF-7 DpVp300 cells have significant changes in gene expression

To determine which genes might be involved in romidepsin resistance, we assessed changes in gene expression between the MCF-7 and MCF-7 DpVp300 cells as well as between the

HuT78 parental and HuT78 DpVp50 resistant cell line that we previously generated (17). We observed significant changes in steady-state mRNA levels between the sensitive and resistant lines for both pairs (Figure 2A, Supplemental Table S3A and S3B). Approximately 500 genes were upregulated, and 180 genes were downregulated (|l2fc| > 1.0 and padj < 0.05) in both HuT78 and MCF-7 DpVp cells (Figure 2B). The majority of the GO-terms enriched for up- or down-regulated genes were distinct between the two cell line pairs and offered no indication of shared molecular pathways that could drive resistance to romidepsin (Supplemental Table S3A). As expected, we observed little change in the expression level of *ABCB1* mRNA. One of the most highly upregulated genes in both resistant cell lines was METTL7A, a putative methyltransferase (Figure 2B). METTL7B, a paralog of METTL7A, is an alkyl-thiol methyltransferase that is capable of methylating thiol-containing compounds such as captopril (18). As the active form of romidepsin contains a thiol as the zinc binding group, and as methylation of romidepsin has been shown to inactivate the molecule (9), we hypothesized that METTL7A might drive resistance in DpVp cells by methylating and inactivating romidepsin. Immunoblot analysis confirmed high levels of METTL7A protein not only in MCF-7 DpVp300 and HUT78 DpVp50 cells but also in another resistant cell line, HuT78 DpP75 (17) (Fig. 2C). Taken together, these results indicate that METTL7A is upregulated in MCF-7 DpVp300, HuT78 DpVp50 and HuT78 DpP75 cells and may play a role in romidepsin resistance.

METTL7A is upregulated at the transcriptional level

To determine if METTL7A is regulated at the level of transcription, we compared chromatin accessibility in the sensitive and DpVp lines for MCF-7 and HuT78. We identified a total of 19,937 differentially open regions (DORs) (padj < 0.05) in the MCF-7 cells and 34,737 DORs in the HuT78 cells (Figure 2D, Supplemental Table S3C). Consistent with our observation that there is little overlap between up- and down-regulated genes at the mRNA level, we observed little overlap between MCF-7 and HuT78 DpVp DORs, with only 737 DORs common to both DpVp cell lines (Figure 2E). *De novo* motif discovery of transcriptional binding sites at DORs shows little overlap between the two cell lines, (Supplemental Figure S3B), suggesting different transcriptional networks are active in the two DpVp cell lines. As expected, genes associated with highly accessible DORs tend to be upregulated in the DpVp cells (Figure 2F). Finally, upregulation of METTL7A is associated with open DORs at the genomic locus (Figure 2G) and an increase in density of subnucleosomal DNA fragments (Supplemental Figure S3C). In both the MCF-7 and HuT78 cell lines, we identified potential binding sites at the METTL7A promoter region for transcription factors that are over expressed in the DpVp cells (Supplemental Table S3D and S3E).

MCF-7 DpVp300 cells are resistant to other thiol-based HDACIs

If we are correct in our assumption that METTL7A can methylate and inactivate HDACis with a thiol as the zinc-binding group, MCF-7 DpVp300 cells should be resistant to other HDACis with a thiol group. Cytotoxicity assays were next performed on MCF-7 and MCF-7 DpVp300 cells with several thioester prodrugs that hydrolyze to yield a thiol as the zinc-binding group: largazole, a natural-product HDACi (32); OKI-005, an HDACi based on the structure of largazole and related to the HDACi OKI-179 that is currently in clinical

trials (19,33); KD5170, a class I and II HDACi (34); and NCH-51, an HDACi based on the structure of vorinostat, except that the zinc-binding hydroxamic acid moiety is replaced with a thiol (35). We found that the DpVp300 cells were resistant to all the thiol-based HDACis tested (Supplemental Figure S4A and Supplemental Table S4). Furthermore, we observe that when cells are treated with these thiol-based HDACis, expression of acetylated histone H3 and p21 expression increased in MCF-7 cells but not the DpVp300 cells (Supplemental Figure S4B). This suggests that MCF-7 DpVp300 cells are selectively resistant to the effects of thiol-based HDACis and supports the hypothesis that METTL7A methylates and inactivates thiol-based HDACis, driving resistance to treatment.

Knockout of METTL7A in MCF-7 DpVp300 cells restores sensitivity to thiol-based HDACis

To investigate whether METTL7A was responsible for the observed resistance to thiol-containing HDACis, we performed CRISPR-Cas9-mediated knockout of *METTL7A*. We generated two clones that were completely negative for METTL7A expression, as well as one clone with reduced expression but not total loss of METTL7 protein (Figure 3A). After a 24 h treatment with 10 ng/ml romidepsin, we found that the ability of romidepsin to induce histone H3 acetylation and p21 was restored in the complete knockouts while little effect was observed in the clone with partial knockdown (Figure 3A). In agreement with this observation, sensitivity to romidepsin was restored nearly to the level of parent MCF-7 cells in the knockout clones, while resistance to the HDACis was only slightly decreased in the partial knockdown clone (Figure 3B). Loss of METTL7A also restored sensitivity to KD-5170, largazole, NCH-51, or OKI-005 (Figure 3B, Supplemental Table S5). Sensitivity to vorinostat, which does not contain a thiol group, was unchanged (Supplemental Table S5).

In agreement with the cytotoxicity data and the effects on histone H3 acetylation and p21 expression (Figure 3C), we observed significant cell cycle perturbations after treatment with the thiol-based HDACis in both METTL7A knockout clones, comparable to what we observed with MCF-7 cells. In the partial knockout clone, we noted some significant cell-cycle changes; however, these changes were less pronounced compared to MCF-7 cells, suggesting that even a low level of METTL7 expression is still protective to the cells (Figure 3D, Supplemental Figure S5). These results all pointed to METTL7A as a mediator of resistance to HDACis with a thiol as the zinc-binding moiety.

Overexpression of METTL7A or METTL7B confers resistance to thiol-based HDACis

To further test the ability of METTL7A to confer resistance to thiol-containing HDACis, METTL7A and METTL7B were overexpressed in HEK-293 cells, which are sensitive to HDACis (Figure 4A). Three-day cytotoxicity assays were performed on the transfected cells with largazole, OKI-005, romidepsin, NCH-51 or KD5170 along with two non-thiol HDAC inhibitors, vorinostat and mocetinostat. METTL7A overexpression conferred resistance to all thiol-based HDACis, but not to the non-thiol HDAC inhibitors, vorinostat and mocetinostat (Figure 4B and Supplemental Table S6). METTL7B overexpression conferred minimal resistance to romidepsin and it also appeared to be less effective than METTL7A for largazole and KD5170 (Figure 4B).

In agreement with cytotoxicity assays, cells expressing METTL7B displayed increased levels of acetylated histone H3 and p21 after treatment with romidepsin, while cells expressing METTL7A were resistant to the effects of all the thiol-based HDACis (Figure 4C). Furthermore, no significant cell cycle changes were observed after treatment with thiol-based HDACis in cells overexpressing METTL7A. In METTL7B expressing cells, while no significant cell cycle changes were observed with a majority of the thiol-based HDACs, we did note significant cell cycle perturbations in cells treated with romidepsin and KD-5170 (Figure 4D, Supplemental Figure S6).

Evidence of methylated romidepsin in culture medium

If METTL7A can methylate romidepsin, we rationalized that we should observe methylated romidepsin in the culture medium of MCF-7 DpVp300 cells incubated with the drug, since this has been demonstrated for other METTL7A substrates (36). Using liquid-chromatography coupled to tandem-mass spectrometry (LC-MS/MS) we observed high levels of dimethylated romidepsin in the media of MCF-7 DpVp300 cells (Figure 5A), whereas much lower levels were observed in the media of MCF-7 cells and the two METTL7A knockout clones, supporting the hypothesis that METTL7A can methylate and inactivate romidepsin.

The ability of METTLA and METTL7B to methylate romidepsin was also examined in a cell-free system. Recombinant METTL7A and METTL7B were incubated with reduced romidepsin. Both METTL7A and METTL7B were found to monomethylate reduced romidepsin (Figure 5B). In contrast, no methylated product, or trace amounts was noted when the reactions were performed in the absence of the methyl donor S-adenosyl-L-methionine (SAM), or when the enzyme was inactivated by pre-treatment with boiling. Together, these results confirm the methyltransferase activity of these enzymes using romidepsin as a substrate.

The phenylethanolamine-N-methyltransferase inhibitor DCMB was recently reported to selectively inhibit the activity of METTL7A but not METTL7B (36). We therefore conducted cytotoxicity assays in cells overexpressing METTL7A, combining DCMB with NCH-51 or romidepsin. Using a non-toxic concentration of DCMB (100 μM) we found that DCMB completely reversed resistance to NCH-51 mediated by METTL7A (Figure 5C) but not romidepsin, where only a slight effect was observed (Figure 5D). The latter observation could be due to the fact that METTL7A has a higher affinity for romidepsin than DCMB. Inhibitors of other methyltransferases may also be potential inhibitors of METTL7A and METTL7B and may reverse resistance to thiol-based HDACis.

Normal tissue expression of METTL7A and METTL7B

While our work implicates METTL7A in resistance to HDACis, its physiological role in development and homeostasis remains to be determined. Public data from the Human Protein Atlas indicates that METTL7A is highly expressed in liver hepatocytes and a similar pattern was found for METTL7B, although single-cell RNA-seq data suggests that METTL7B is more enriched in proximal enterocytes (37,38). In agreement, immunohistochemistry on normal tissue microarrays showed METTL7A and METTL7B to

be highly expressed in hepatocytes (Figure 6A and 6B, respectively) and distinct segments of the nephron (Figure 6C and 6D). Additionally, METTL7A was found in breast epithelium (Figure 6E and 6F) and is also highly expressed in glial cells and Leydig cells of the testes (Supplemental Table S7). METTL7B was found in intestinal enterocytes (Figure 6G and 6H) as well as enterocytes and neurons (Supplemental Table S7). Finally, modest expression of both METTL7A and METTL7B is also found in cardiomyocytes, gastric mucosa, and subcutaneous adipocytes (Supplemental Table S7). The localization pattern of METTL7A and METTL7B is consistent with a role in detoxification, which might have treatment implications for drugs in this class.

Expression of METTL7A and METTL7B in T-cell lymphoma samples

To explore a potential role for METTL7A or METTL7B in resistance to thiol-based HDAC inhibitors, we obtained a T-cell lymphoma tissue microarray and stained for METTL7A and METTL7B by immunohistochemistry. Of the 52 PTCL samples on the microarray, five (10%) were positive for METTL7A, eight (15%) were positive for METTL7B while two samples (4%) were positive for both proteins. Anaplastic large cell lymphoma and NK/T-cell lymphomas had higher positivity rates, but there were fewer samples on the array compared to T-cell lymphoma. Staining for METLL7A was typically minimal to mild while METLL7B staining was mild to moderate. Positivity rates are summarized in Supplemental Table S8.

DISCUSSION

HDACis are a novel class of chemotherapeutic drugs that modulate histone acetylation by coordinating with Zn^{2+} to inhibit HDACs, thus inhibiting enzyme activity. Vorinostat and romidepsin were the first FDA-approved HDACis for the treatment of T-cell lymphomas (3-5,39). Despite dramatic responses in some patients, romidepsin is not always effective and resistance can develop. While elevated levels of the efflux pump P-gp are associated with *in vitro* resistance to romidepsin, this mechanism does not translate to the clinic (16). Thus, we set out to identify mechanisms of resistance to HDACis. Here, we identify overexpression of the putative methyltransferases METTL7A and METTL7B as a mechanism of drug resistance to thiol-based HDACis in vitro (Figure 6I). METTL7B (18), and more recently METTL7A (36), have been identified as thiol methyltransferases. These enzymes methylate the zinc-coordinating thiol to prevent the drug from inhibiting HDACs, thus conferring resistance to this class of agents. Cells selected for high levels of resistance to romidepsin are also resistant, albeit to a lesser extent, to other HDACis that do not contain thiol groups. This suggests that one or more factors in the resistant cells promote more general resistance to HDACis. Whether these are mediated by some of the other molecular changes we have observed in these cells remains to be determined.

Few studies have linked expression of METTL7A or METTL7B to drug resistance. Jun and colleagues identified METTL7A as a mechanism of resistance in methotrexate resistant choriocarcinoma cells (40). However, we did not find increased resistance to methotrexate in the DpVp300 line. We note that methotrexate does not contain a thiol moiety, suggesting that other factors besides METTL7A may be involved in methotrexate resistance in their

model. A role for METTL7B in resistance to tyrosine kinase inhibitors (TKIs) has been suggested by Song and colleagues who noted increased expression of METTL7B in lung adenocarcinoma cell lines that were resistant to gefitinib or osimertinib (41). They observed METTL7B did not directly interact with the TKIs, but rather METTL7B overexpression was associated with increased antioxidant capacity and reactive oxygen species (ROS) scavenging (41).

The observation that both METTL7A and METTL7B were able to methylate romidepsin in a cell-free system contrasts with the findings from our cell line models which suggest that METTL7A is the relevant driver of resistance to romidepsin. Several reasons can explain this discrepancy and warrant further investigation. Differences in protein structure, reaction site preferences, post-translational modifications, binding partners, or sub-cellular localization between the two enzymes could all result in differences in activity toward romidepsin.

While our work reveals a role for METTL7A and METTL7B in drug resistance, the physiological role of these methyltransferases remains to be elucidated. One of the murine homologs of METTL7A, Mettl7a1, is transiently and significantly upregulated during reprogramming of mouse embryonic fibroblasts (MEFs) to induce endoderm progenitors (42). Addition of Mettl7a1 to the reprogramming cocktail enhanced conversion of MEFs into induced endoderm progenitors by promoting reprogramming efficiency. METTL7A also plays a role in osteogenic differentiation by mediating the effects of glucose on cell survival and osteogenic induction (43). Lastly, both METTL7A and METTL7B have been proposed to play a role in hydrogen sulfide homeostasis (18,36). Both paralogs are expressed in the stomach, kidney, and liver which may suggest a detoxifying role for these proteins under normal physiological conditions. METTL7A has also recently been localized to Bergmann glia, suggesting a potential role in the CSF-brain barrier (44).

While we are not able to provide formal evidence that expression of METTL7A in tumors is a mechanism of resistance to romidepsin, our data showing expression of METTL7A and METTL7B in 10% and 15% of peripheral T-cell lymphoma, respectively, supports a potential role in clinical resistance to thiol-based HDACis. However, further clinical studies are required to determine the prevalence of this mechanism of resistance among romidepsin treated patients. Additionally, expression of METTL7A or METTL7B in the tumor may not be the only factor that determines the role of METTL7A or METTL7B clinical response to thiol-based HDACis. The high levels of METTL7A and METTL7B expressed in the liver may result in systemic resistance by inactivating the drugs circulating in the blood stream before the drug reaches the tumor cells. We previously found that histone H3 acetylation of peripheral blood mononuclear cells 24 h after administration of romidepsin was associated with response (16), which may indicate the need for increased drug exposure. As patients with higher levels of METTL7A in the liver may be systemically exposed to less drug, this could result in a poorer response. However, further experiments will be required to dissect the contribution of METTL7A and METTL7B to drug metabolism. We hope that the information presented here will encourage and facilitate future clinical studies to determine if there is a role for METTL7A and METTL7B expression in clinical drug resistance to thiol-containing HDACis.

The data presented here show that METTL7A can inactivate thiol-containing HDACis before they reach their targets. It is possible that this mechanism of resistance, despite the potential to reduce effective drug concentrations in cancer cells, also reduces the systemic effects of the drugs given to patients. A key challenge in oncopharmacology is that we do not always know if a drug has reached its target. How much the presence of METTL7A is responsible for the inability to translate the unique activity seen in T-cell lymphomas to solid tumors remains to be investigated (45-48). While this paper supports a role for METTL7A in the emergence of resistance in T-cell lymphomas, the clinical relevance of this observation remains to be proven. These findings are a reminder of just how much remains to be learned and solved regarding how cancers become resistant to treatment.

Supplementary Material

Refer to Web version on PubMed Central for supplementary material.

ACKNOWLEDGEMENTS

We thank members of the Batista, Gottesman and Arda Labs for discussion and critical reading of the manuscript. The authors thank the Center for Cancer Research (CCR) Genomics Core in Bethesda, Maryland, as well as the CCR Sequencing Facility in Frederick, Maryland, for help with high-throughput sequencing. This work utilized the computational resources of the NIH HPC Biowulf cluster (http://hpc.nih.gov). We appreciate the editorial assistance of George Leiman. The views expressed in this article are those of authors and may not reflect the official policy or position of the National Institute of Health, Department of the Army, Department of Defense. Mention of trade names, commercial products, or organizations imply endorsement by the U.S. Government. This work is supported by the Intramural Research Program at the National Cancer Institute (NCI) of the National Institutes of Health. C.M.F. is partially supported by a Postdoctoral Fellowship from the American Cancer Society (PF-19-157-01-RMC). A.K.T. is supported by Department of Defense – BCRP Level 2 award (1W81XWH-21-1-0053). This work was supported in part by National Institutes of Health National Institute of General Medical Sciences [Grant T32-GM007750] (to D.A.R.) and National Heart, Lung, and Blood Institute [Grant R01-HL146603].

List of Abbreviations

5-FU	5-fluorouracil
AcH3	Acetylated Histone H3
ATAC-seq	Assay for transposase-accessible chromatin with sequencing
CCR	Center for Cancer Research, National Cancer Institute
DCMB	2,3-dichloro-alpha-methylbenzylamine
DIPEA	N,N-Di-isoproylethylamine
DMPG	1,2-Dimyristoyl-sn-glycero-3-phospho-rac-(1-glycerol) sodium salt
DOR	Differentially open regions of chromatin
DpVp	Cells treated with romidepsin in the presence of the inhibitor verapamil
FDA	Food and Drug Administration
H3	Histone H3

HAT	Histone acetyltransferase
HDAC	Histone deacetylase
HDACi	Histone deacetylase inhibitor
P-gp	P-glycoprotein
PAGE	poly acrylamide gel electrophoresis
PBS	phosphate buffered saline
PTCL	peripheral T-cell lymphoma
RNA-seq	RNA sequencing
SAM	S-adenosyl-L-methionine
TCEP	tris(2-carboxyethyl)phosphine
TMA	Tissue Microarray

REFERENCES

1. Bates SE. Epigenetic Therapies for Cancer. N Engl J Med 2020;383(7):650–63 doi 10.1056/NEJMra1805035. [PubMed: 32786190]
2. Robey RW, Chakraborty AR, Basseville A, Luchenko V, Bahr J, Zhan Z, Bates SE. Histone deacetylase inhibitors: emerging mechanisms of resistance. Mol Pharm 2011;8(6):2021–31 doi 10.1021/mp200329f. [PubMed: 21899343]
3. Duvic M, Talpur R, Ni X, Zhang C, Hazarika P, Kelly C, et al. Phase 2 trial of oral vorinostat (suberoylanilide hydroxamic acid, SAHA) for refractory cutaneous T-cell lymphoma (CTCL). Blood 2007;109(1):31–9. [PubMed: 16960145]
4. Olsen E, Kim Y, Kuzel T, Pacheco T, Foss F, Parker S, et al. Phase IIb multicenter trial of vorinostat in patients with persistent, progressive, or treatment refractory cutaneous T-cell lymphoma. J Clin Oncol 2007;25(21):3109–15. [PubMed: 17577020]
5. Whittaker SJ, Demierre MF, Kim EJ, Rook AH, Lerner A, Duvic M, et al. Final results from a multicenter, international, pivotal study of romidepsin in refractory cutaneous T-cell lymphoma. J Clin Oncol 2010;28(29):4485–91 doi JCO.2010.28.9066 [pii] 10.1200/JCO.2010.28.9066. [PubMed: 20697094]
6. Piekarz R, Frye R, Turner M, Wright J, Allen S, Kirschbaum M, et al. Phase II multi-institutional trial of the histone deacetylase inhibitor romidepsin as monotherapy for patients with cutaneous T-cell lymphoma. J Clin Oncol 2009;27(32):5410–7. [PubMed: 19826128]
7. O'Connor OA, Horwitz S, Masszi T, Van Hoof A, Brown P, Doorduijn J, et al. Belinostat in Patients With Relapsed or Refractory Peripheral T-Cell Lymphoma: Results of the Pivotal Phase II BELIEF (CLN-19) Study. J Clin Oncol 2015;33(23):2492–9 doi 10.1200/JCO.2014.59.2782. [PubMed: 26101246]
8. Shi Y, Dong M, Hong X, Zhang W, Feng J, Zhu J, et al. Results from a multicenter, open-label, pivotal phase II study of chidamide in relapsed or refractory peripheral T-cell lymphoma. Ann Oncol 2015;26(8):1766–71 doi 10.1093/annonc/mdv237. [PubMed: 26105599]
9. Furumai R, Matsuyama A, Kobashi N, Lee KH, Nishiyama M, Nakajima H, et al. FK228 (depsipeptide) as a natural prodrug that inhibits class I histone deacetylases. Cancer Res 2002;62(17):4916–21. [PubMed: 12208741]
10. Grant S, Dai Y. Histone deacetylase inhibitors and rational combination therapies. Adv Cancer Res 2012;116:199–237 doi 10.1016/B978-0-12-394387-3.00006-9. [PubMed: 23088872]

11. Lee JS, Paull K, Alvarez M, Hose C, Monks A, Grever M, et al. Rhodamine efflux patterns predict P-glycoprotein substrates in the National Cancer Institute Drug Screen. Mol Pharmacol 1994;46:627–38. [PubMed: 7969041]
12. Robey RW, Zhan Z, Piekarz RL, Kayastha GL, Fojo T, Bates SE. Increased MDR1 expression in normal and malignant peripheral blood mononuclear cells obtained from patients receiving depsipeptide (FR901228, FK228, NSC630176). Clin Cancer Res 2006;12(5):1547–55. [PubMed: 16533780]
13. Tabe Y, Konopleva M, Contractor R, Munsell M, Schober W, Jin L, et al. Up-regulation of MDR1 and induction of doxorubicin resistance by histone deacetylase inhibitor depsipeptide (FK228) and ATRA in acute promyelocytic leukemia cells. Blood 2006;107(4):1546–54. [PubMed: 16223781]
14. Xiao JJ, Foraker AB, Swaan PW, Liu S, Huang Y, Dai Z, et al. Efflux of depsipeptide FK228 (FR901228, NSC-630176) is mediated by P-glycoprotein and multidrug resistance-associated protein 1. J Pharmacol Exp Ther 2005;313(1):268–76. [PubMed: 15634944]
15. Yamada H, Arakawa Y, Saito S, Agawa M, Kano Y, Horiguchi-Yamada J. Depsipeptide-resistant KU812 cells show reversible P-glycoprotein expression, hyper-acetylated histones, and modulated gene expression profile. Leuk Res 2006;30(6):723–34. [PubMed: 16260035]
16. Bates S, Zhan Z, Steadman K, Obrzut T, Luchenko V, Frye R, et al. Laboratory correlates for a phase II trial of romidepsin in cutaneous and peripheral T-cell lymphoma. Br J Haematol 2010;148(2):256–67. [PubMed: 19874311]
17. Chakraborty AR, Robey RW, Luchenko VL, Zhan Z, Piekarz RL, Gillet JP, et al. MAPK pathway activation leads to Bim loss and histone deacetylase inhibitor resistance: rationale to combine romidepsin with an MEK inhibitor. Blood 2013;121(20):4115–25 doi 10.1182/blood-2012-08-449140. [PubMed: 23532732]
18. Maldonato BJ, Russell DA, Totah RA. Human METTL7B is an alkyl thiol methyltransferase that metabolizes hydrogen sulfide and captopril. Sci Rep 2021;11(1):4857 doi 10.1038/s41598-021-84218-5. [PubMed: 33649426]
19. Diamond JR, Pitts TM, Ungermannova D, Nasveschuk CG, Zhang G, Phillips AJ, et al. Preclinical Development of the Class-I-Selective Histone Deacetylase Inhibitor OKI-179 for the Treatment of Solid Tumors. Mol Cancer Ther 2022;21(3):397–406 doi 10.1158/1535-7163.MCT-21-0455. [PubMed: 34965958]
20. Liu X, Phillips AJ, Ungermannova D, Nasveschuk CG, Zhang G; Macrocyclic compounds useful as inhibitors of histone deacetylases. US patent US 8754050 B2. 2014 2011/05/26.
21. Ungermannova D. P27 as a molecular target for cancer therapeutics: Discovering small molecule inhibitors of p27 proteolysis and structure-activity relationship and mechanistic studies of largazole, a potent inhibitor of histone deacetylase. University of Colorado-Boulder, Boulder, CO, USA 2010.
22. Corces MR, Trevino AE, Hamilton EG, Greenside PG, Sinnott-Armstrong NA, Vesuna S, et al. An improved ATAC-seq protocol reduces background and enables interrogation of frozen tissues. Nat Methods 2017;14(10):959–62 doi 10.1038/nmeth.4396. [PubMed: 28846090]
23. Smith JP, Corces MR, Xu J, Reuter VP, Chang HY, Sheffield NC. PEPATAC: an optimized pipeline for ATAC-seq data analysis with serial alignments. NAR Genom Bioinform 2021;3(4):lqab101 doi 10.1093/nargab/lqab101. [PubMed: 34859208]
24. Heinz S, Benner C, Spann N, Bertolino E, Lin YC, Laslo P, et al. Simple combinations of lineage-determining transcription factors prime cis-regulatory elements required for macrophage and B cell identities. Mol Cell 2010;38(4):576–89 doi 10.1016/j.molcel.2010.05.004. [PubMed: 20513432]
25. Weirauch MT, Yang A, Albu M, Cote AG, Montenegro-Montero A, Drewe P, et al. Determination and inference of eukaryotic transcription factor sequence specificity. Cell 2014;158(6):1431–43 doi 10.1016/j.cell.2014.08.009. [PubMed: 25215497]
26. Bankhead P, Loughrey MB, Fernandez JA, Dombrowski Y, McArt DG, Dunne PD, et al. QuPath: Open source software for digital pathology image analysis. Sci Rep 2017;7(1):16878 doi 10.1038/s41598-017-17204-5. [PubMed: 29203879]

27. Richon VM, Sandhoff TW, Rifkind RA, Marks PA. Histone deacetylase inhibitor selectively induces p21WAF1 expression and gene-associated histone acetylation. Proc Natl Acad Sci U S A 2000;97(18):10014–9. [PubMed: 10954755]
28. Sandor V, Robbins AR, Robey R, Myers T, Sausville E, Bates SE, Sackett DL. FR901228 causes mitotic arrest but does not alter microtubule polymerization. Anticancer Drugs 2000;11(6):445–54. [PubMed: 11001385]
29. Landreville S, Agapova OA, Matatall KA, Kneass ZT, Onken MD, Lee RS, et al. Histone deacetylase inhibitors induce growth arrest and differentiation in uveal melanoma. Clin Cancer Res 2012;18(2):408–16 doi 10.1158/1078-0432.CCR-11-0946. [PubMed: 22038994]
30. Bernhart E, Stuendl N, Kaltenegger H, Windpassinger C, Donohue N, Leithner A, Lohberger B. Histone deacetylase inhibitors vorinostat and panobinostat induce G1 cell cycle arrest and apoptosis in multidrug resistant sarcoma cell lines. Oncotarget 2017;8(44):77254–67 doi 10.18632/oncotarget.20460. [PubMed: 29100385]
31. Piekarz RL, Robey RW, Zhan Z, Kayastha G, Sayah A, Abdeldaim AH, et al. T-cell lymphoma as a model for the use of histone deacetylase inhibitors in cancer therapy: impact of depsipeptide on molecular markers, therapeutic targets, and mechanisms of resistance. Blood 2004;103(12):4636–43. [PubMed: 14996704]
32. Liu Y, Salvador LA, Byeon S, Ying Y, Kwan JC, Law BK, et al. Anticolon cancer activity of largazole, a marine-derived tunable histone deacetylase inhibitor. J Pharmacol Exp Ther 2010;335(2):351–61 doi 10.1124/jpet.110.172387. [PubMed: 20739454]
33. Wang X, Waschke BC, Woolaver RA, Chen Z, Zhang G, Piscopio AD, et al. Histone Deacetylase Inhibition Sensitizes PD1 Blockade-Resistant B-cell Lymphomas. Cancer Immunol Res 2019;7(8):1318–31 doi 10.1158/2326-6066.CIR-18-0875. [PubMed: 31235619]
34. Hassig CA, Symons KT, Guo X, Nguyen PM, Annable T, Wash PL, et al. KD5170, a novel mercaptoketone-based histone deacetylase inhibitor that exhibits broad spectrum antitumor activity in vitro and in vivo. Mol Cancer Ther 2008;7(5):1054–65 doi 10.1158/1535-7163.MCT-07-2347. [PubMed: 18483295]
35. Suzuki T, Nagano Y, Kouketsu A, Matsuura A, Maruyama S, Kurotaki M, et al. Novel inhibitors of human histone deacetylases: design, synthesis, enzyme inhibition, and cancer cell growth inhibition of SAHA-based non-hydroxamates. J Med Chem 2005;48(4):1019–32 doi 10.1021/jm049207j. [PubMed: 15715470]
36. Russell DA, Chau MK, Shi Y, Levasseur IN, Maldonato BJ, Totah RA. METTL7A (TMT1A) and METTL7B (TMT1B) are responsible for alkyl S-thiol methyl transferase activity in liver. Drug Metab Dispos 2023 doi 10.1124/dmd.123.001268.
37. Uhlen M, Fagerberg L, Hallstrom BM, Lindskog C, Oksvold P, Mardinoglu A, et al. Proteomics. Tissue-based map of the human proteome. Science 2015;347(6220):1260419 doi 10.1126/science.1260419. [PubMed: 25613900]
38. Karlsson M, Zhang C, Mear L, Zhong W, Digre A, Katona B, et al. A single-cell type transcriptomics map of human tissues. Sci Adv 2021;7(31) doi 10.1126/sciadv.abh2169.
39. Piekarz RL, Frye R, Prince HM, Kirschbaum MH, Zain J, Allen SL, et al. Phase 2 trial of romidepsin in patients with peripheral T-cell lymphoma. Blood 2011;117(22):5827–34 doi 10.1182/blood-2010-10-312603. [PubMed: 21355097]
40. Jun F, Peng Z, Zhang Y, Shi D. Quantitative proteomic analysis identifies novel regulators of methotrexate resistance in choriocarcinoma. Gynecol Oncol 2020 doi 10.1016/j.ygyno.2020.01.013.
41. Song H, Liu D, Wang L, Liu K, Chen C, Wang L, et al. Methyltransferase like 7B is a potential therapeutic target for reversing EGFR-TKIs resistance in lung adenocarcinoma. Mol Cancer 2022;21(1):43 doi 10.1186/s12943-022-01519-7. [PubMed: 35144642]
42. Biddy BA, Kong W, Kamimoto K, Guo C, Waye SE, Sun T, Morris SA. Single-cell mapping of lineage and identity in direct reprogramming. Nature 2018;564(7735):219–24 doi 10.1038/s41586-018-0744-4. [PubMed: 30518857]
43. Lee E, Kim JY, Kim TK, Park SY, Im GI. Methyltransferase-like protein 7A (METTL7A) promotes cell survival and osteogenic differentiation under metabolic stress. Cell Death Discov 2021;7(1):154 doi 10.1038/s41420-021-00555-4. [PubMed: 34226523]

44. Vera-Montecinos A, Galiano-Landeira J, Roldan M, Vidal-Domenech F, Claro E, Ramos B. A Novel Localization of METTL7A in Bergmann Glial Cells in Human Cerebellum. Int J Mol Sci 2023;24(9) doi 10.3390/ijms24098405.

45. Otterson GA, Hodgson L, Pang H, Vokes EE, B CaLG. Phase II study of the histone deacetylase inhibitor Romidepsin in relapsed small cell lung cancer (Cancer and Leukemia Group B 30304). J Thorac Oncol 2010;5(10):1644–8 doi 01243894-201010000-00024 [pii] 10.1097/JTO.0b013e3181ec1713. [PubMed: 20871263]

46. Whitehead R, Rankin C, Hoff P, Gold P, Billingsley K, Chapman R, et al. Phase II trial of romidepsin (NSC-630176) in previously treated colorectal cancer patients with advanced disease: a Southwest Oncology Group study (S0336). Invest New Drugs 2009;27(5):469–75. [PubMed: 18941712]

47. Stadler WM, Margolin K, Ferber S, McCulloch W, Thompson JA. A phase II study of depsipeptide in refractory metastatic renal cell cancer. Clinical Genitourinary Cancer 2006;5(1):57–60. [PubMed: 16859580]

48. Molife L, Attard G, Fong P, Karavasilis V, Reid A, Patterson S, et al. Phase II, two-stage, single-arm trial of the histone deacetylase inhibitor (HDACi) romidepsin in metastatic castration-resistant prostate cancer (CRPC). Ann Oncol 2010;21(1):109–13. [PubMed: 19608618]

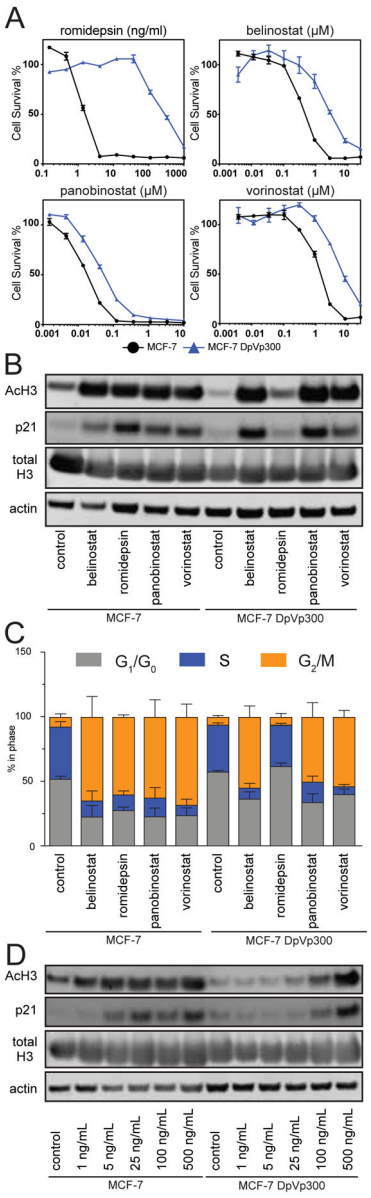

Figure 1. MCF-7 DpVp300 cells are selectively resistant to romidepsin.

(A) Three-day cytotoxicity assays were performed on MCF-7 cells (black circles) and MCF-7 DpVp300 cells (blue triangles) with the histone deacetylase inhibitors romidepsin, belinostat, panibinostat and vorinostat.

(B) MCF-7 and MCF-7 DpVp300 cells were plated and allowed to attach overnight. Cells were subsequently treated with belinostat (5 μM), romidepsin (10 ng/ml), panobinostat (5 μM), or vorinostat (5 μM) for 24 h after which protein was extracted and subjected to immunoblot analysis. Membranes were incubated with antibodies to pan acetylated histone H3 (AcH3), total histone H3 (total H3), p21 or actin. One of three independent experiments is shown.

(C) MCF-7 and MCF-7 DpVp300 cells were plated and allowed to attach overnight after which cells were exposed to belinostat (5 μM), romidepsin (10 ng/ml), panobinostat (5 μM),

or vorinostat (5 μM) for 24 h. Cells were subsequently analyzed by flow cytometry and the percentage of cells in each phase of the cell cycle was determined using ModFit LT v 5.0. The graph was generated from data compiled from three independent experiments. Error bars are standard deviation.

(D). MCF-7 and MCF-7 DpVp300 cells were plated and allowed to attach overnight after which cells were exposed to increasing concentrations of romidepsin for 24 h. After harvesting cells and subjecting extracted protein to immunoblot analysis, proteins were probed with antibodies as described in (B). One of three independent experiments is shown.

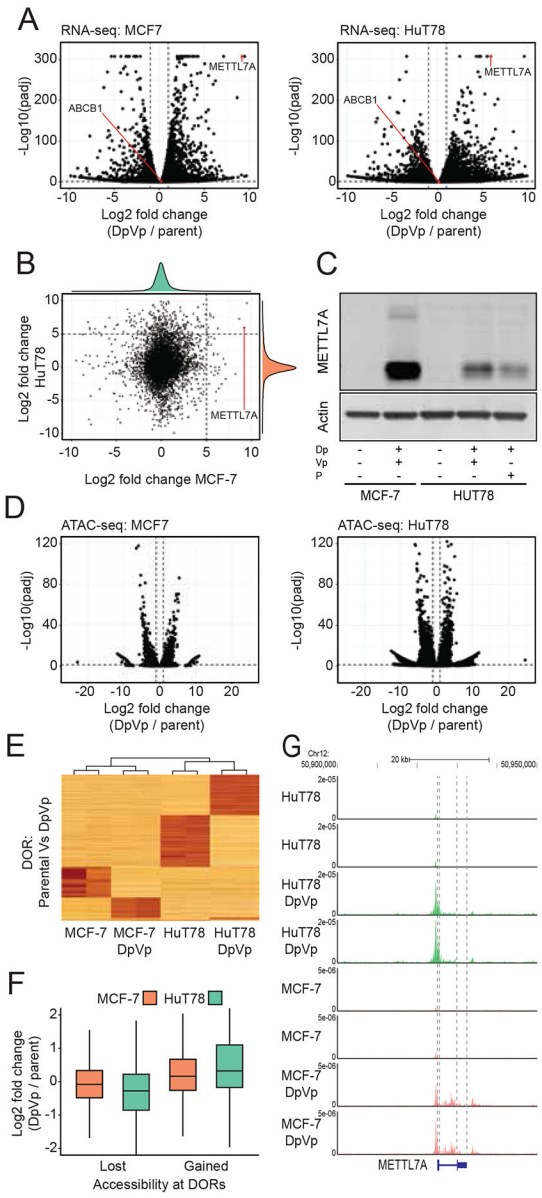

Figure 2. RNA-seq and ATAC-seq analysis of MCF-7 and MCF-7 DpVp300 cells.

(A) Volcano plot depicting steady state fold change in mRNA levels between MCF-7 and MCF-7 DpVp300 (left) and HuT78 and HuT78 DpVp50 (right). Changes in gene expression were determined with DEseq2. The drug efflux gene *ABCB1* and *METTL7A* are indicated with a red line.

(B) Scatterplot depicting the log2 fold change of transcripts in MCF-7 and MCF-7 DpVp300 compared to the log2 fold change in HuT78 and HuT78 DpVp50 cells. A log2 fold change of 5 is indicated on the x and y-axis with a dashed line. *METTL7A* is indicated with a red line.

(C) Immunoblot of METTL7A in the MCF-7 and HuT78 resistance models.

(D) Volcano plot depicting the fold change of differentially open regions in MCF7 cells (left) and HuT78 cells (right) identified with PEPATAC.

(E) Heatmap depicting changes in the differentially open regions in MCF-7, MCF-7 DpVp300, HuT78 and HuT78 DpVp50 cells.
(F) Box plot showing log2 fold change in mRNA levels for genes linked to differentially open region that gain or lose accessibility in DpVp cells. Genes linked to differentially open regions with both gain and loss of accessibility are excluded.
(G) Differentially open regions at the genomic locus of METTL7A in MCF-7, MCF-7 DpVp300, HuT78, and HuT78 DpVp50 cells.

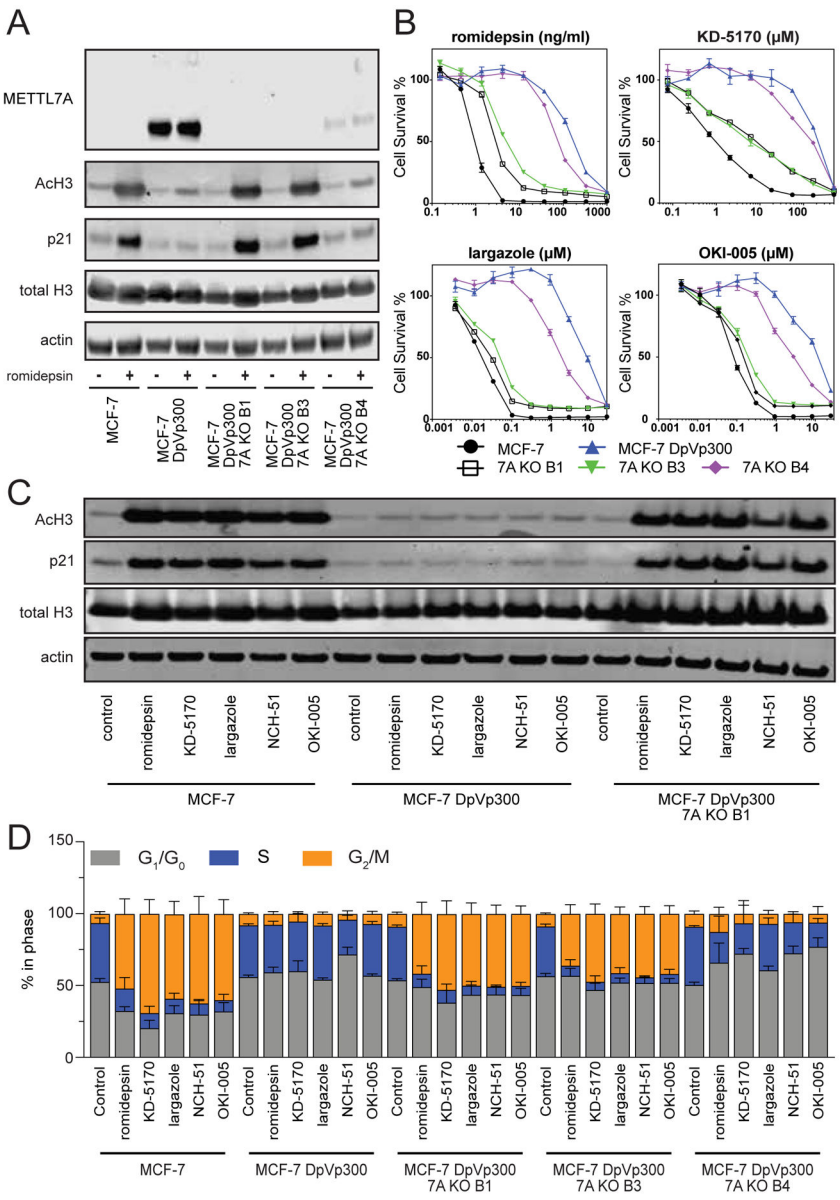

Figure 3. Deletion of METTL7A restores sensitivity to thiol-based HDACIs in MCF-7 DpVp300 cells

(A) MCF-7 and MCF-7 DpVp300 cells, as well as knockout clones (7A KO B1 and 7A KO B3) and partial knockdown clone 7A KO B4 were plated and allowed to attach overnight. Cells were subsequently left untreated or treated with romidepsin (10 ng/ml) for 24 h. After harvesting cells and subjecting extracted protein to PAGE, proteins were transferred to nitrocellulose that was probed with METTL7A antibody as well as pan acetylated histone H3 (AcH3), total histone H3 (total H3), p21 or actin antibodies.

(B) Three-day cytotoxicity assays were performed with romidepsin, KD-5170, largazole, NCH-51, OKI-005 and vorinostat on MCF-7 cells (black circles), MCF-7 DpVp300 cells (blue triangles), 7A KO B1 cells (open black squares), 7A KO B3 (inverted green triangles) and 7A KO B4 (purple diamonds).

(C) MCF-7, MCF-7 DpVp300 and 7A KO B1 cells were plated and allowed to attach overnight. Cells were subsequently treated with romidepsin (10 ng/ml), KD-5170 (10 μM), largazole (250 nM), NCH-51 (25 μM), or OKI-005 (500 nM) for 24 h after which protein was extracted and subjected to PAGE. Proteins were transferred to nitrocellulose membranes and blots were incubated with antibodies to pan acetylated histone H3 (AcH3), total histone H3 (total H3), p21 or actin. Results from one of three independent experiments is shown. (D) MCF-7, MCF-7 DpVp300 and 7A KO B1 cells were plated and allowed to attach overnight after which cells were exposed to belinostat (5 μM), romidepsin (10 ng/ml), panobinostat (5 μM), or vorinostat (5 μM) for 24 h. Cell cycle analysis was subsequently performed and the percentage of cells in each phase was determined using ModFit LT v 5.0. The graph was generated from data compiled from three independent experiments. Error bars indicate standard deviation.

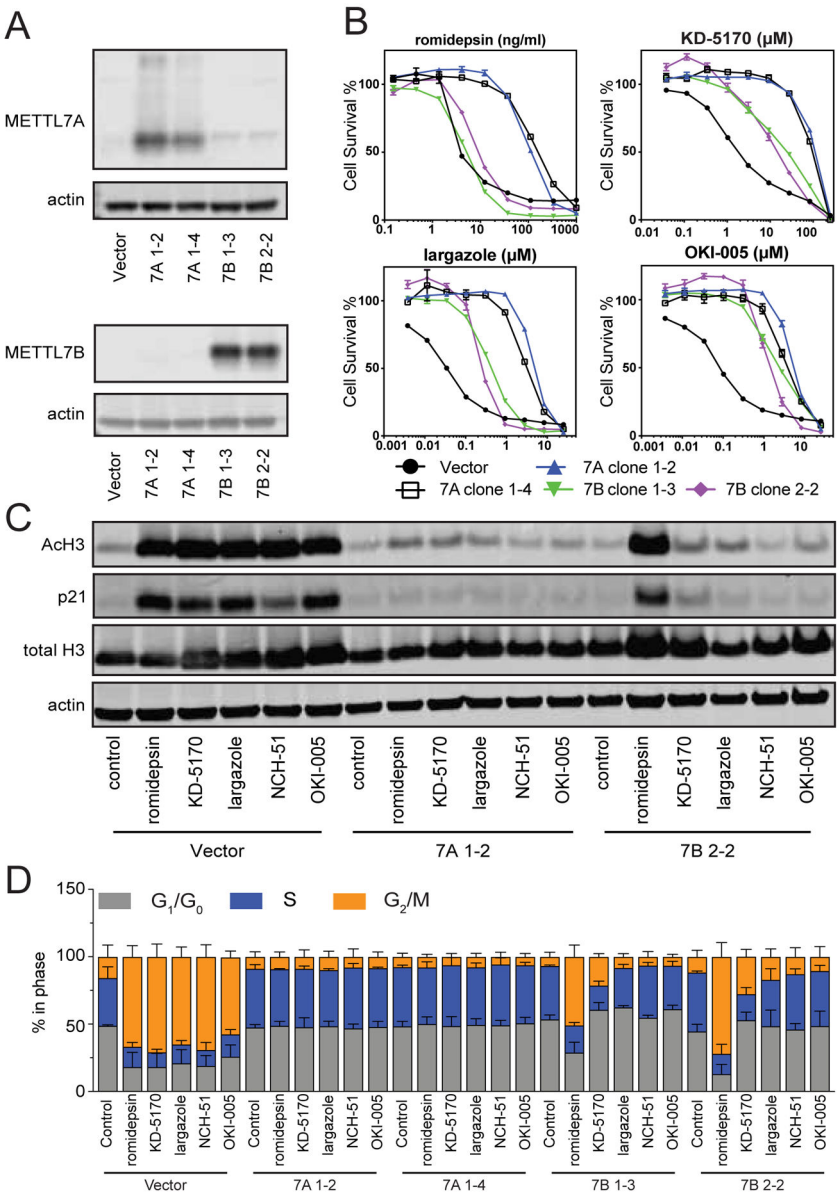

Figure 4. METTL7A and METTL7B overexpression confers varying levels of resistance to thiol-based HDACis.

(A) HEK293 cells were transfected with empty vector (vector) or with vector encoding METTL7A (clones 7A 1-2 and 7A 1-4) or METTL7B (clones 7B 1-3 and 7B 2-2). Proteins were extracted and subjected to immunoblot. The blots were probed with antibodies to METTL7A, METTL7B or actin.

(B) Three-day cytotoxicity assays were performed with romidepsin, KD-5170, largazole, or OKI-005 on empty vector (vector) cells (black circles), 7A 1-2 cells (blue triangles), 7A 1-4 cells (open black squares), 7B 1-3 (inverted green triangles) and 7B 2-2 (purple diamonds).

(C) Empty vector (vector) cells, 7A 1-2 cells, 7A 1-4 cells, 7B 1-3 cells, and 7B 2-2 cells were plated and treated with romidepsin (10 ng/ml), KD-5170 (10 μM), largazole (250 nM), NCH-51 (25 μM), or OKI-005 (500 nM) for 24 h after which protein was extracted and subjected to PAGE. Proteins were transferred to nitrocellulose membranes and blots were

incubated with antibodies to pan acetylated histone H3 (AcH3), total histone H3 (total H3), p21 or actin. Results from one of three independent experiments is shown.
(D) Empty vector (vector) cells, 7A 1-2 cells, 7A 1-4 cells, 7B 1-3 cells, and 7B 2-2 cells were plated and treated with romidepsin (10 ng/ml), KD-5170 (10 μM), largazole (250 nM), NCH-51 (25 μM), or OKI-005 (500 nM) for 24 h after which cell cycle analysis was performed. The percentage of cells in each phase was determined using ModFit LT v 5.0. The graph was generated from data compiled from 3 independent experiments. Error bars indicate standard deviation.

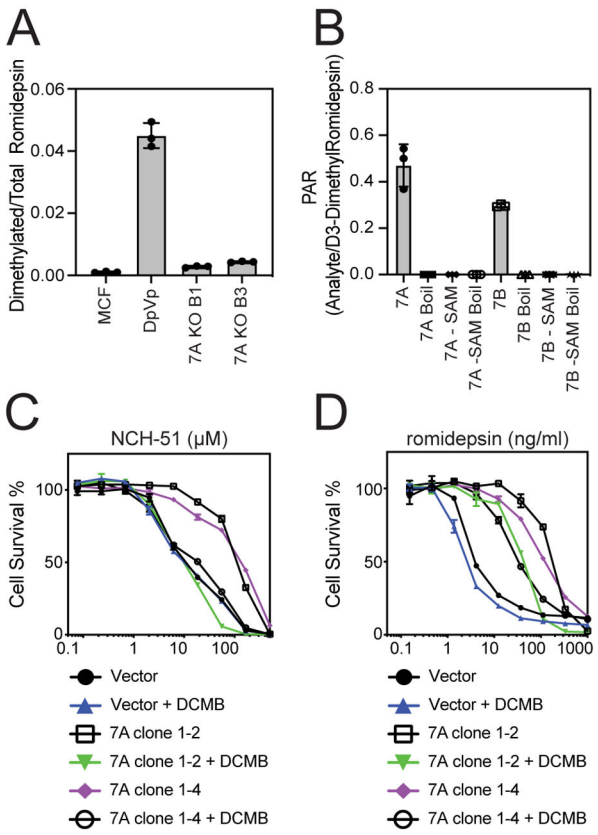

Figure 5. METTL7A methylation of romidepsin *in vitro*

(A) Measurement of dimethylated romidepsin by LC-MS/MS in cell culture media following 24 h of incubation with MCF-7, MCF-7 DpVp300, 7A KO B1 and 7A KO B3 cells.

(B) Measurement of methylated romidepsin with METTL7A and METTL7B in a cell-free system. Methylation reactions were carried out with recombinant enzyme and the amount of methylated product was measured by LC-MS/MS. Omission of the methyl donor SAM, and boiling the enzyme were used as controls.

(C) Three-day cytotoxicity assays were performed with NCH-51 on empty vector (vector) cells (black circles), empty vector cells with 100 μM DCMB (blue triangles), 7A 1-2 cells (open black squares), 7A 1-2 cells with 100 μM DCMB (inverted green triangles) 7A 1-4 cells (purple diamonds), and 7A 1-2 cells with 100 μM DCMB (open black circles).

(D) Three-day cytotoxicity assays were performed as noted above in (C), except romidepsin was used instead of NCH-51.

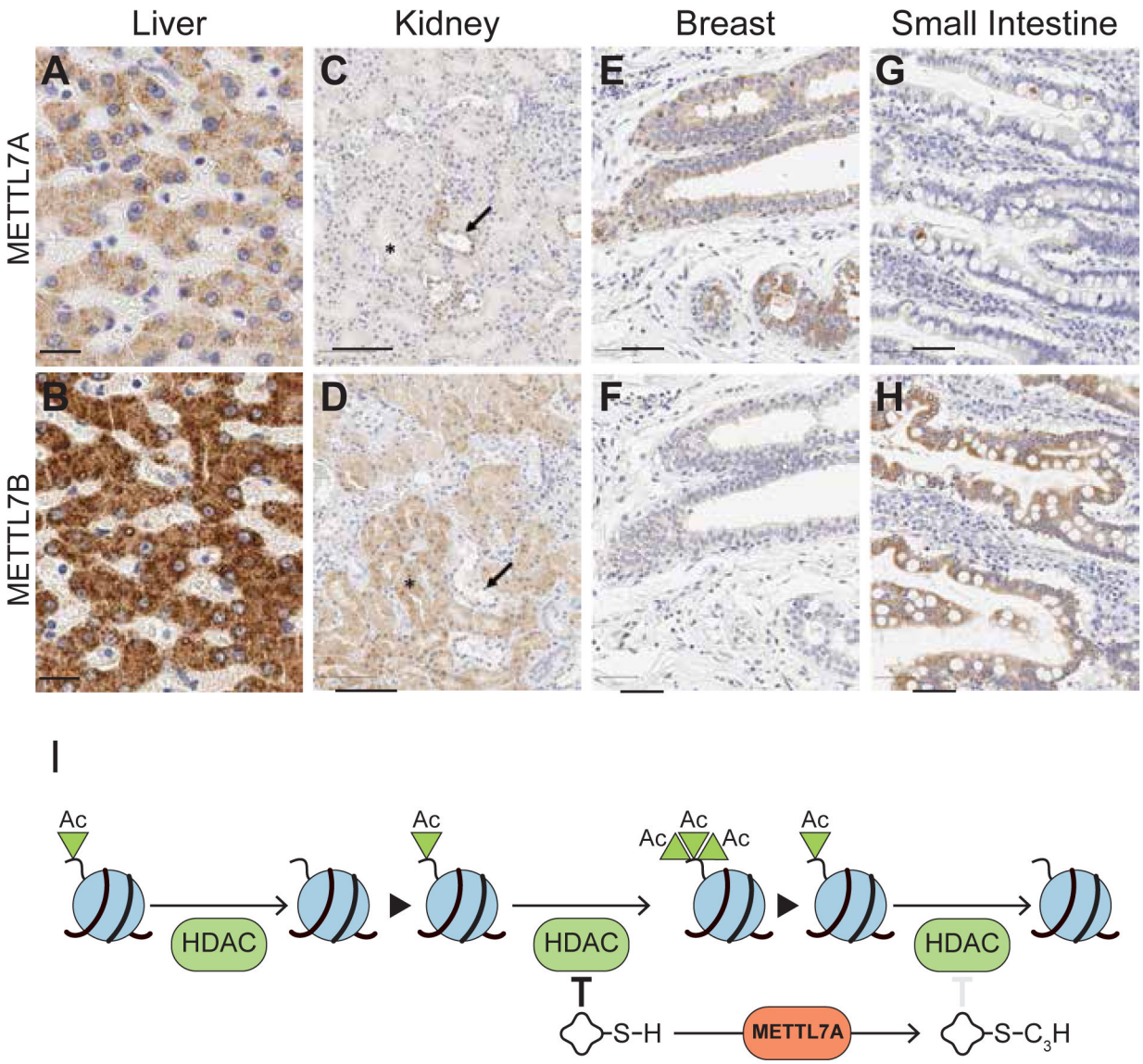

Figure 6: Normal and tumor tissue expression of METTL7A and METTL7B and proposed model

Normal tissue expression of METTL7A and METTL7B. A strong cytoplasmic pattern is observed in hepatocytes (A and B), distinct regions of the nephron (C and D), breast epithelium (E and F), and small intestinal enterocytes (G and H). Arrows and asterisks indicate distinct METTL7A and METTL7B expression patterns in renal tubules on serial sections. Scale bars represent 20 μm (A and B), 100 μm (C and D), and 50 μm (E, F, G, and H). (I) Proposed model of drug resistance through activity of METTL7A.